ACS Catalysis

Research Article

pubs.acs.org/acscatalysis

Nitrogen-Rich Mesoporous Carbons: Highly Efficient, Regenerable Metal-Free Catalysts for Low-Temperature Oxidation of H_2S

Fugen Sun,‡ Jun Liu,‡ Huichao Chen, Zixiao Zhang, Wenming Qiao, Donghui Long,* and Licheng Ling

State Key Laboratory of Chemical Engineering, East China University of Science and Technology, Shanghai, China

Supporting Information

ABSTRACT: We demonstrate that it is possible to transform traditional mesoporous carbons into a superior metal-free catalyst for low-temperature H_2S removal via doping a high concentration of nitrogen atoms into the carbon. The nitrogen doping level is important for the activity of mesoporous carbons as a metal-free catalyst. Although carbons doped with only an intermediate amount of nitrogen (e.g., 4.3 wt %), show little aptitude for the catalytic oxidation of H_2S when nitrogen doping reaches a certain high level (e.g., 8.5 wt %), the nitrogen-rich mesoporous carbons (NMC) exhibit high catalytic activity and selectivity toward H_2S oxidation at low temperature. Further study suggests that the pyridinic nitrogen atoms are responsible for the catalytic activity in H_2S oxidation. Owing to the metal-free nature of the NMC catalyst, it can be easily regenerated by CS_2 scrubbing, and the product sulfur can be recovered. Our desulfurization results suggest that such metal-free carbons could, indeed, overcome the limitations of the conventional H_2S catalysts and provide suitable, sustainable, and inexpensive solutions for technological development in H_2S removal.

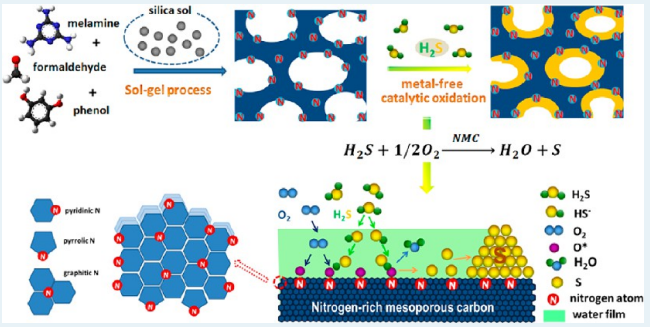

KEYWORDS: *Mesoporous carbon, nitrogen doping, metal-free catalysis, catalytic oxidation, H_2S removal*

1. INTRODUCTION

Removal of H_2S is one of the most important technologies for the utilization of gasified products from many industrial processes, such as natural gas processing, biogas purification, petroleum refining, petrochemical plants, coke ovens, and coal gasifiers.[1] General methods of H_2S removal include amine aqueous solution,[2] adsorption-clause process,[3] biological methods,[4] and fixed-bed solid catalytic oxidation processes.[5] From the viewpoint of environmental and cost concerns, low-temperature direct oxidation of H_2S to elemental sulfur by the use of a selective oxidation catalyst is the preferred approach for dilute H_2S-containing gas streams.[6,7] The selective oxidation of H_2S has the thermodynamic potential to remove H_2S to the parts-per-billion level, even at very low temperature. This technology can be easily integrated into the current fuel processing plants. It can be used with diverse gas streams, and it does not consume H_2 or other useful gas components.[7]

As for the catalysts, activated carbons have been shown to be one of most suitable candidates, especially working at low temperature.[8−11] Their use in partial oxidation of H_2S has been identified as a highly promising approach for removing sulfur content in various gas flues. This is the result of unique properties of activated carbons, such as large surface area, and high pore volume as well as their rich surface chemistry.[12,13] To further improve their catalytic activity and kinetics of reaction, they are generally impregnated with caustic materials such as NaOH or Na_2CO_3, or other pH-control agents;[14−17] however, pores act as storage spaces for oxidation products, such as elemental sulfur.

An intrinsic problem of activated carbons is their small micropore size and low pore volume that cannot accommodate a mass of solid sulfur. Therefore, the sulfur capacity of caustic impregnated activated carbon desulfurizer was limited to 0.2−0.6 g H_2S/g catalyst. The relatively low sulfur saturation capacity necessitated the frequent replacement of these catalysts, increasing the operation cost and limiting their applicability. Recently, we found that use of impregnated mesoporous carbon aerogels instead of activated carbons could greatly overcome this problem.[18,19] The ultrahigh catalytic activity (up to 2.5 g H_2S/g catalyst) of impregnated carbon aerogels was attributed to the large pore volume and 3-dimensional mesoporosity of the carbon, which allow easy diffusion and storage of reactants and products. Although caustic impregnated carbon aerogels have been reported as effective H_2S catalysts for low-temperature oxidation of H_2S, there are still some inherent disadvantages: (i) a low self-ignition temperature due to the alkali impregnation, (ii) the special precaution required to be used with alkalis, and (iii) the difficulty of regeneration. Better adsorbents that, with sustained efficiency and regenerability, would be much safer to employ are thus required.

Received: December 6, 2012
Revised: March 19, 2013
Published: March 26, 2013

Surface chemistry is an important factor governing the catalytic properties of carbons, so great efforts have been paid to development of metal-free carbon catalysts by introducing basic nitrogen-containing functional groups.[20−25]Nitrogen could introduce basic/catalytic sites to the carbon, which can increase surface polarity and enhance electron-donor properties of the carbon matrix and, in turn, increase the chemical reactivity for acid−base or redox chemistry.[24,25]Nitrogen-doped activated carbons have been commercialized to act as adsorbents for adsorption of H_2S. The nitrogen-induced basic environment favors the dissociation of H_2S and the oxidation of H_2S in the presence of water.[11] However, nitrogen-doped activated carbons still have a lower market share than impregnated activated carbons.[26−28] This could be due to their surface chemistry, which does not enhance the specific adsorption and catalytic processes. Thus, to develop an advanced and green catalyst for H_2S removal, both high surface density of catalytic sites for catalytic activity and high pore volume for sulfur storage are necessary.

Herein, we report the surprisingly high catalytic activity of nitrogen-rich mesoporous carbons (NMC) for the direct oxidation of H_2S into elemental sulfur at room temperature. The NMC catalysts are prepared by a conventional colloidal silica nanocasting process using phenol−melamine−formaldehyde resin as a nitrogen-enriched carbon precursor. Features of the as-prepared NMC, including high nitrogen content (up to 8 wt %) and developed mesoporous structure, led to high catalytic activity and selectivity toward H_2S oxidation, consistent with our goals in designing advanced H_2S catalysts. Furthermore, we demonstrate that the nitrogen doping level is important for the activity of mesoporous carbons as a metal-free catalyst for H_2S removal. The pyridinic nitrogen atoms are proposed to be responsible for the catalytic activity in the H_2S oxidation. Owing to the metal-free nature of NMC, the exhausted catalyst can be easily regenerated by CS_2 scrubbing or thermal sublimation. Our results suggest that such nitrogen-rich carbons could provide suitable, sustainable, and inexpensive solutions for the technological development in H_2S removal.

2. EXPERIMENTAL SECTION

2.1. Preparation. The NMC were synthesized via a colloidal silica-assisted sol−gel process, using phenol, melamine, and formaldehyde as carbon precursor.[29] In a typical synthetic procedure, 3.67 g phenol (39 mmol) and 6.33 g formaldehyde (37 wt %, 78 mmol) were dissolved in 50 mL of 0.2 M NaOH solution (10 mmol). The mixture was stirred at 70 oC for 40 min. Then, 4.92 g melamine (39 mmol) and 9.50 g formaldehyde (107 mmol) were added to the above solution to react for 30 min with consecutive agitation until the solution became clear. Next, 50 g Ludox SM-30 sol (30 wt % SiO_2) was added to the above solution under stirring. The mixture was transferred to a sealed bottle and heated at 80 °C for 3 days. The obtained hydrogels were directly dried at 80 °C in an ambient condition, followed by the carbonization at 800 °C for 3 h with a heating rate of 5 °C/min in a nitrogen flow. The NMC were obtained by dissolution of the silica nanoparticles in 2 M NaOH solution at 80 °C, isolated by filtration, washed with distilled water until the pH did not change, and dried at 100 °C. In this work, the initial weight ratio of polymer (phenol, formaldehyde, and melamine) to colloidal silica was fixed at 1:1, whereas the mole ratio of melamine to phenol was changed from 0 to 2. The as-prepared NMC samples were denoted as M/P-*x*, where *x* represents the mole ratio of melamine to phenol.

In addition, a series of NMC with different carbonization temperatures was also prepared using the same polymer precursor of M/P-1. Here, the M/P-1 precursor was heated at a designed temperature (700, 800, 900, 1000 °C) for 3 h at a heating rate of 5 °C/min in nitrogen flow. The as-prepared samples are denoted as M/P-1-*x*, where x represents the carbonization temperature.

A commercial catalyst, caustic impregnated activated carbon catalyst (JT3018, supplied by Purit Chemical Corp. Ltd.), is also used for H_2S oxidation.

2.2. Catalytic Test. The NMC (particle size: 30−50 mesh) were packed in a glass tube with a diameter of 4 mm and a height of 20 mm. Humidified air containing 1000 ppmv of H_2S (relative humidity 80%) was passed through the column of the NMC (0.3 g) at a flow rate of 150 mL/min. The gas flow rates were controlled by a mass flow controller system (Aalborg GFM17A). The reaction temperature was controlled by a K-type thermocouple in the furnace and monitored by another K-type thermocouple axially centered in the reactor tube. The concentrations of the exhaust gases from the reactor were monitored using gas chromatography (GC, Shimadzu GC2010) with a pulsed flame photometric detector (FPD) permitting detection levels as low as 0.5 ppm. The test was stopped at the point that the elution concentration was ∼90% to the inlet concentration. In this test, the breakthrough concentration of H_2S was defined as 5 ppm. The sulfur capacity (g of H_2S/g of catalyst) was then calculated by integrating the corresponding breakthrough curves.

2.3. Characterization. Elemental analysis was carried out using Elemental Vario EL III. The carbon (C), hydrogen (H), and nitrogen (N) contents of the carbons were determined directly using the thermal conductivity detector.

The surface composition of the NMC was obtained from an Axis Ultra DLD X-ray photoelectron spectroscopy. The X-ray source operated at 15 kV and 10 mA. The working pressure was lower than 2×10^{-8}Torr. The N1s XPS spectra were measured at 0.1 eV step size. The binding energies were calibrated taking C_{1S} as a standard with a measured typical value of 248.6 eV.[30] The N_{1S} XPS signals were fitted with mixed Lorentzian−Gaussian curves, and a Shirley function was used to subtract the background using a XPS peak processing software.[31−33]

The thermogravimetric analysis (TA Instrument Q600 Analyzer) of samples was carried out at a nitrogen flow rate of 100 mL/min. The samples were heated to 800 °C at a rate of 5 °C/min.

The X-ray diffraction (XRD) patterns were acquired on a Rigaku D/max 2550 diffractometer operating at 40 KV and 20 mA using Cu Kα radiation (λ = 1.5406 Å).

The morphologies of samples were observed under scanning electron microscopy (SEM, JEOL 7100F) and transmission electron microscopy (TEM, JEOL 2100F). The SEM mapping was observed under scanning electron microscopy (SEM, FEI Q-300).

Nitrogen adsorption/desorption isotherms were measured at 77 K with a Quadrasorb SI analyzer. Before the measurements, the NMC samples were degassed in vacuum at 473 K for 12 h, and the exhausted sulfur-containing NMC were degassed in vacuum at 333 K for 24 h. The Brunauer−Emmett−Teller (BET) method was utilized to calculate the specific surface

dx.doi.org/10.1021/cs300791j | ACS Catal. 2013, 3, 862−870

Table 1. Chemical Nature, Pore Parameters and Breakthrough Sulfur Capacities of the NMC

	element analysis		XPS								
samples	N, wt %	N/C, at./at.	N, at. %	N/C, at./at.	pyridinic N[a] %	pyrrolic N[b] %	graphitic N[c] %	S_{BET}[d] m^2/g	V_T[e] cm^3/g	D[f] nm	sulfur capacity[g] g/g
M/P-0								593	1.4	10.2	0.05
M/P-0.5	4.3	0.04	12.5	0.18	56.7	29.7	13.6	777	2.4	10.7	0.17
M/P-1	8.1	0.08	20.4	0.31	56.2	31.7	12.1	731	2.6	10.8	1.85
M/P-2	11.9	0.13	24.5	0.40	54.6	31.3	14.1	770	2.4	10.9	2.77
M/P-1-700	8.6	0.10	20.8	0.32	57.2	32.5	10.3	706	2.5	10.7	1.94
M/P-1-900	6.0	0.07	14.4	0.19	45.4	28.8	24.2	786	2.8	10.7	1.59
M/P-1-1000	5.8	0.06	13.9	0.18	42.5	25.8	33.2	790	2.8	10.6	1.51

[a]The relative concentration of pyridinic N (398.5 ± 0.3 eV). [b]The relative concentration of pyrrolic N (400.5 ± 0.3 eV). [c]The relative concentration of graphitic N (401.6 ± 0.3 eV). [d]BET specific surface area. [e]Total pore volume (P/P_0 = 0.985). [f]BJH desorption average pore size. [g]Breakthrough sulfur capacity.

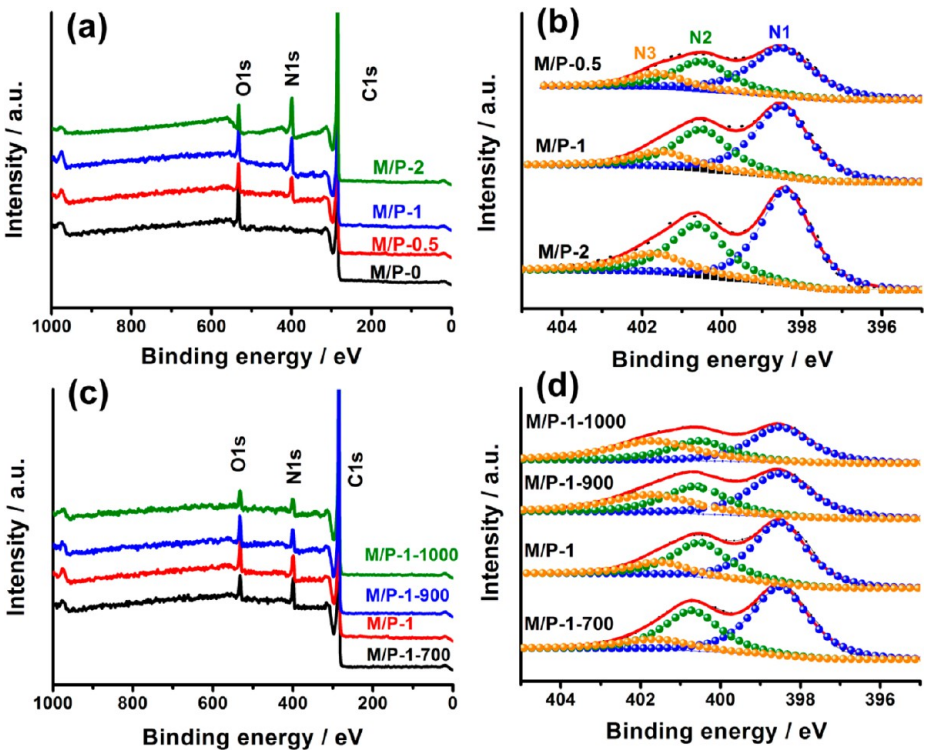

Figure 1. (a) XPS survey and (b) high-resolution N1s spectra of the NMC with different M/P ratios. (c) XPS survey and (d) high-resolution N1s spectra of the M/P-1 prepared at different pyrolysis temperatures.

area. The pore size distributions were derived from desorption branch by using the Barrett–Joyner–Halenda (BJH) model.

3. RESULTS AND DISCUSSION

3.1. Structure and Chemical Nature of the NMC. The NMC catalysts were prepared by a colloidal silica nanocasting process using melamine, phenol, and formaldehyde as the carbon precursor, followed by carbonization of precursor and removal of colloidal silica template. The synthesis was very flexible as a result of the sol–gel process, which permitted the preparation of NMC in different formats (sphere, monolith, etc.),[29] and tailoring their porous texture and chemical nature. Keys to the success of our synthesis approach lie in the incorporation of high-nitrogen-content melamine into phenolic precursors that can transfer nitrogen atoms into the carbon framework under pyrolysis conditions. As shown in Table 1, elemental analysis discloses that the nitrogen content can be tunable over a wide range by changing the initial M/P ratio in the precursors. A higher amount of melamine in M/P-2 precursors leads to a higher nitrogen concentration of 11.9 wt % in the final carbonized structures. This N content is, to our knowledge, comparable to the highest for nitrogen-containing porous carbon materials produced by the direct pyrolysis of nitrogen-rich precursors or through post-treatment of pre-formed carbons.[34,35]The confined effect, facilitated by the colloidal silica nanoparticles, may lead to more N atoms incorporated into the carbon framework. The N content of the NMC is also dependent on the pyrolysis temperature. For the same precursor M/P-1, higher pyrolysis temperature results in lower nitrogen content, as expected.

High-resolution XPS was employed to investigate the elemental composition and N-bonding configurations formed in the surface of the carbon framework. In the range of XPS sensitivity, only carbon, nitrogen, and oxygen are detected in the survey scans (Figure 1a), thus excluding the presence of any other impurities. The highest N/C mole ratio of 0.4 is achieved

dx.doi.org/10.1021/cs300791j | ACS Catal. 2013, 3, 862–870

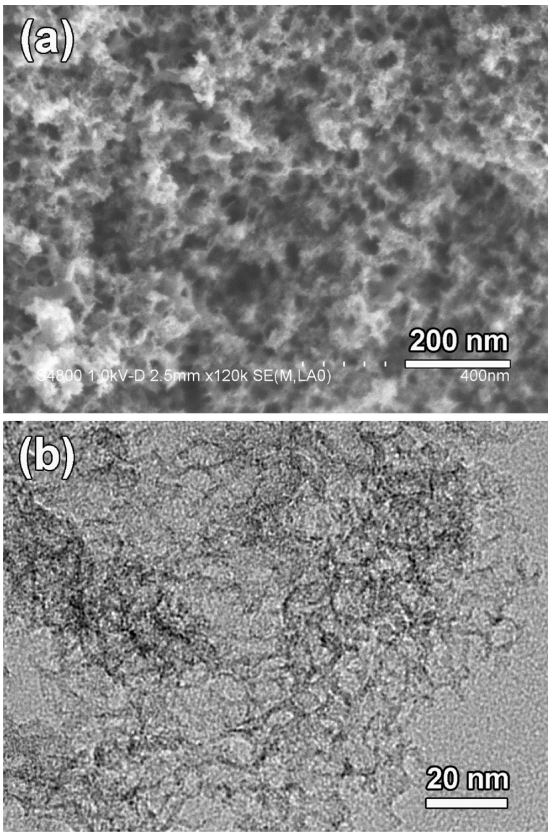

Figure 2. Typical SEM (a) and TEM (b) images of the M/P-2.

at the M/P ratio of 2, three times higher than the value obtained from elemental analysis. The variation of the values can be explained by the surface specificity of XPS measurements, suggesting the N atoms tend to gather at the surface rather than at the bulk of the carbon framework.

The N1s spectra were deconvoluted using mixed Gaussian–Lorentzian component profiles after subtraction of a Shirley background. As shown in Figure 1b, the N1s spectra are curve-fitted into three peaks with binding energies of 398.5 ± 0.3, 400.5 ± 0.3, and 401.6 ± 0.3 eV that correspond to pyridinic N (N1), pyrrolic N (N2), and graphitic N (N3), respectively.[31−33] It is worth noting that +at the same pyrolysis temperature, the distribution of these nitrogen species (Figure 1b, Table 1) is almost similar, regardless of the M/P ratio, even though the M/P ratio is in proportion to the N content (Table 1). However, in the case of the same precursor (M/P-1), the N-bonding configurations could be significantly adjusted via changing the pyrolysis temperature. With an increase in the pyrolysis temperature from 700 to 1000 °C, the relative intensity of pyridinic N decreases while the opposite trend for the graphitic N is observed (Table 1). This result indicates that the pyrolysis temperature is the dominant element in the form of N-bonding configurations.

A representative SEM image of the M/P-2 is shown in Figure 2a, which shows an open 3-D interconnected network composed of mesopores and some macropores, due to the replication of colloidal silica nanoparticles and some coalesced colloidal aggregates. The TEM image (Figure 2b) further indicates that the pore size and connectivity of those NMC exactly reflect the geometric properties of the original template. The well-developed spherical mesopores with an average pore size of ∼10 nm can be regarded as a direct image or, more

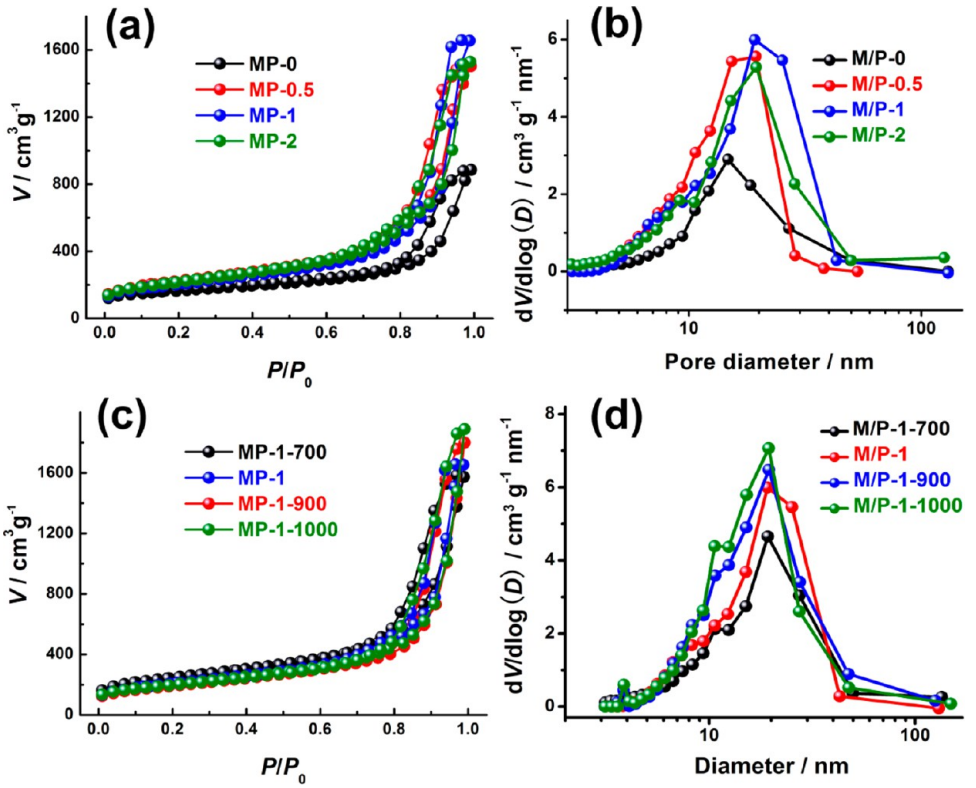

Figure 3. N_2 adsorption–desorption isotherms of the NMC with different M/P ratios (a) and the M/P-1 prepared at different pyrolysis temperatures (b).

dx.doi.org/10.1021/cs300791j | ACS Catal. 2013, 3, 862–870

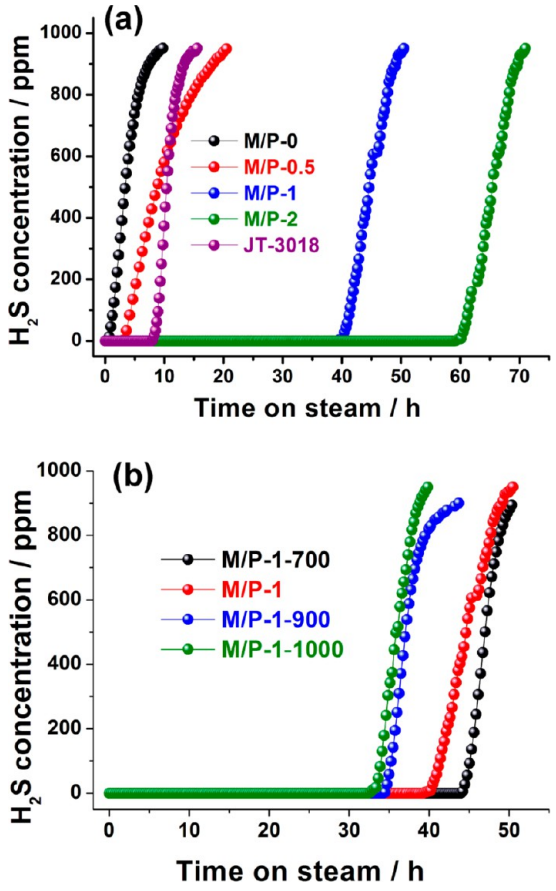

Figure 4. H_2S breakthrough curves over the NMC with different M/P ratios (a) and the M/P-1 with different pyrolysis temperatures (b).

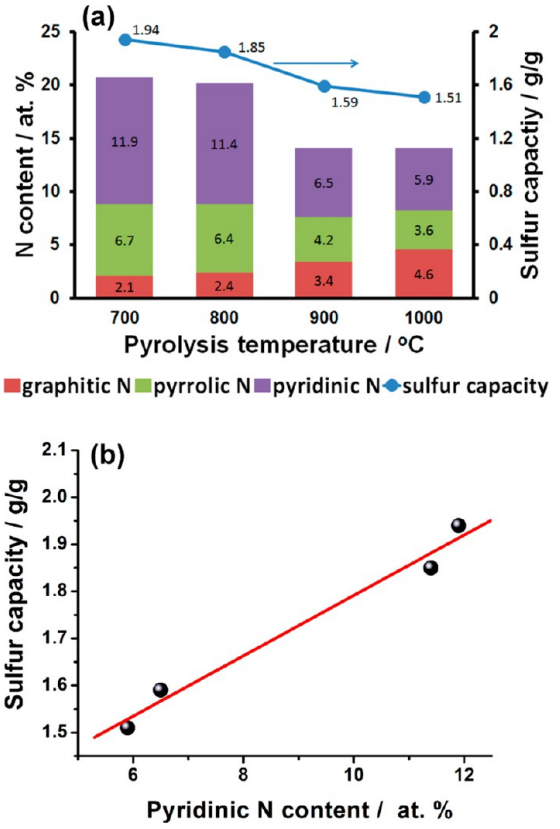

Figure 5. (a) The nitrogen-bonding configurations and breakthrough sulfur capacities of the NMC prepared at different pyrolysis temperatures. (b) Breakthrough sulfur capacity as a function of pyridinic N content.

appropriately, as a negative image of the structure of the colloidal silica particles (7 nm). These results do, indeed, show a structural inversion of the template structure, thus enabling perfect nanocasting and structural control.

The addition of melamine into phenolic precursors could slightly modify the mesoporous structure, possibly as a result of the different carbonization yields of the precursors. As shown in Figure 3a, the obtained NMC have a typical type-IV isotherm with pronounced adsorptions at high relative pressures (0.7−0.9 P/P_0), demonstrating the existence of a large number of mesopores. The BET specific surface areas and total pore volumes of these NMC are in the range of 593−777 m^2/g and 1.4−2.8 cm^3/g, respectively. The mesopore sizes for all samples were in the range of 10−20 nm as a result of the replication of the colloidal silica nanoparticles. Some pores larger than the single silica nanoparticle are often formed because of the presence of coalesced colloidal aggregates.The pyrolysis temperature has a negligible effect on the porosity of the NMC, a fact reflected by their similar N_2 adsorption−desorption isotherms (Figure 3b). The detailed porosity parameters are summarized in Table 1.

3.2. Metal-Free Catalytic Oxidation of H_2S over the NMC. The metal-free catalytic properties of these NMC toward H_2S oxidation were tested in a packed-bed reactor under atmospheric pressure at a temperature of 30 °C and weight hourly space velocity of 5.5 h^{-1}. Figure 4 depicts the H_2S breakthrough curves on the NMC with different nitrogen contents. From the curves, the breakthrough capacities are listed in Table 1. Notably, the NMC catalysts with low or intermediate nitrogen content (e.g., 4.3 wt % for M/P-0.5) show negligible catalytic activity. When the nitrogen content in NMC is up to 8 wt %, however, the desulfurization activity greatly increases. Unprecedented breakthrough sulfur capacities, as high as 1.85 g/g and 2.77 g/g, are obtained for the samples NMC (M/P-1) and NMC (M/P-2), respectively. Such values are almost 5−8 times higher than that of the commercial caustic desulfurizer JT3108 (0.36 g/g), which is widely used in the H_2S removal industry. To our knowledge, such a huge breakthrough sulfur capacity is among the highest sulfur capacities reported to date.[18] It is noted that the M/P-0.5 and M/P-2 have almost the same mesoporous structure; however, their completely different catalytic activities are obviously due to higher nitrogen content for the latter. This result indicates that there is a critical value in nitrogen content or carbon surface basicity, which when exceeded results in an unprecedented metal-free catalytic activity for H_2S oxidation.

Since nitrogen content certainly plays an important role in the H_2S oxidation and at least three different forms of the surface nitrogen atoms have been observed, it is important to understand the effect of the nitrogen chemical state on the metal-free catalytic performance. In Figure 4b, we compare the catalytic properties of the M/P-1 samples prepared at different pyrolysis temperatures. These samples have similar mesoporous structures. Their primary differences are a different nitrogen content and their distributions of nitrogen species present. As shown in Table 1, the breakthrough sulfur capacity gradually decreases from 1.94 to 1.51 g/g when the pyrolysis temperature is increased from 700 to 1000 °C. The reason is apparently due

dx.doi.org/10.1021/cs300791j | ACS Catal. 2013, 3, 862−870

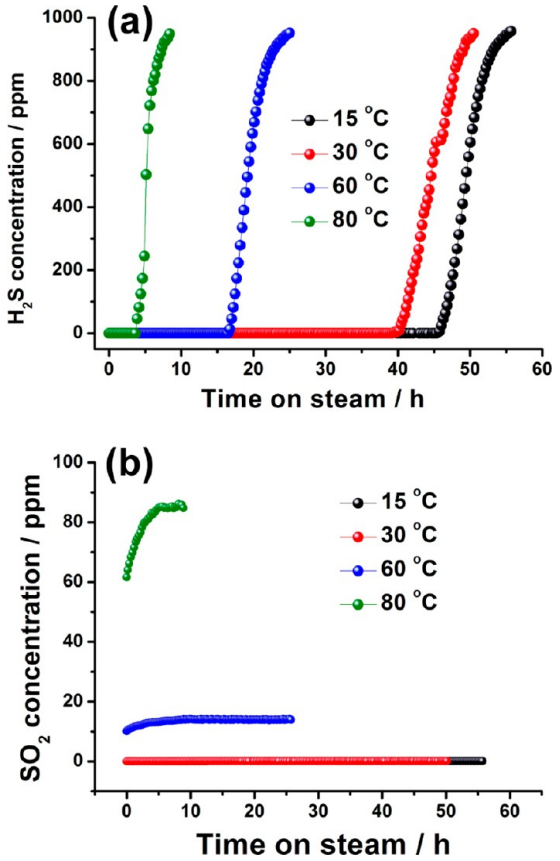

Figure 6. The H_2S (a) and SO_2 (b) breakthrough curves of the M/P-1 at different working temperatures.

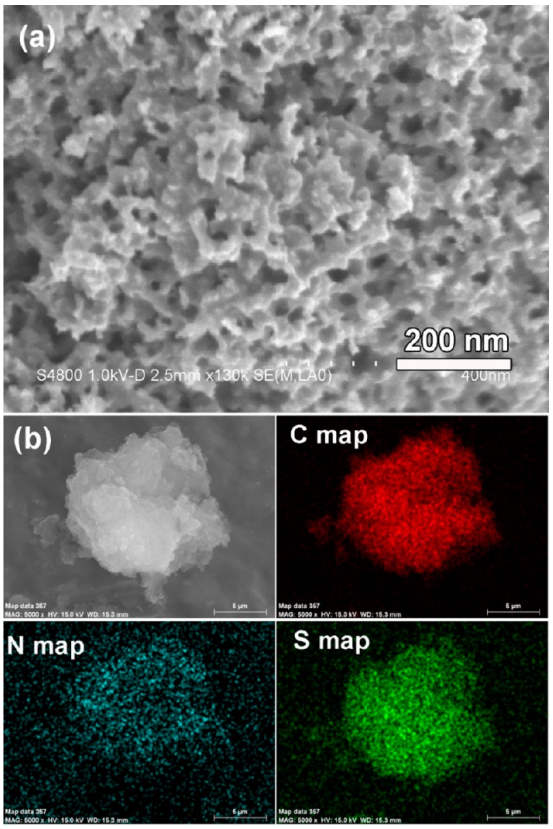

Figure 7. SEM image (a) and SEM mapping (b) of the M/P-2 after the metal-free catalytic oxidation of H_2S at 30 °C.

to the various nitrogen contents in the NMC. Furthermore, in association with our XPS analysis of the NMC, the content of pyridinic N is largely decreased while that of graphitic N slightly increases with an increase in the pyrolysis temperature (Figure 5a). We thus correlate the relationship between pyridinic N content and the sulfur capacity and find a good linear dependence between them (Figure 5b). Therefore, it is reasonable to believe that the pyridinic N is accountable for the catalytic activity. Given that pyridinic N atoms located at the edges of graphene sheets have strong electron-accepting ability, they are favorable for the adsorption of oxygen atoms, thus facilitating the oxidation reaction. In fact, these pyridinic nitrogen atoms were also reported to be the most active for catalysis in oxygen reduction reaction[36] and sulfur dioxide removal.[37] Thus, it is not only the nitrogen content but also the nitrogen bonding configurations (especially pyridinic nitrogen) that could be the key to implementing the metal-free catalytic activity of the carbon. Further work on the precise role of the nitrogen in the catalytic oxidation of H_2S is ongoing.

Tail gases from the outlet of the reactor, including H_2S, COS, and SO_2 were continuously monitored by a residual gas analyzer to determine the selectivity of H_2S oxidation. At the low temperature range (30 °C) for the oxidation experiments, no COS and SO_2 are detected in the column effluent for all samples, indicating the excellent selectivity (almost 100%) for oxidation of H_2S to elemental sulfur via the reaction $H_2S + 1/2O_2 \rightarrow S + H_2O$. This observation is confirmed after the good agreement found between the amounts of sulfur removed from the effluent and the formed elemental sulfur in the exhausted solids, as determined by mass balance calculation and TG analysis (Figure S1 in Supporting Information).

The working temperature is further investigated from 15 to 80 °C for NMC (M/P-1) as shown in Figure 6. Low temperature is found to be favorable for highly efficient oxidation of H_2S. An increase of the working temperature (60−80 °C) is deleterious not only on the catalytic activity but also on the selectivity. An increase in the reaction temperature may lead to SO_2 formation via a deep oxidation reaction, $2H_2S + 3O_2 \rightarrow 2SO_2 + 2H_2O$, resulting in a decrease in the oxidation selectivity. An increase in the working temperature causes a decrease in the catalytic activity of the NMC, possibly due to the weakened capability of adsorbing the reactants (e.g., O_2).[38] In addition, it may also be linked to the breaking of the water film on the carbon surface at high reaction temperature in the present of humidity. Further investigation of the temperature effects should be carried out in the future.

3.3. Product Analysis of H_2S Oxidation over the NMC.

The product, elemental sulfur, was directly deposited in the mesopores of NMC, which could be easily observed by SEM (Figure 7a). The formed sulfur is found to be homogenously deposited in the carbon framework, rather than forming sulfur agglomerations filled in pores. No discernible sulfur particles are found in the pores of NMC throughout the SEM and TEM observations (Figure S2−S4, Supporting Information). The sulfur and carbon elemental mapping (Figure 7b) further demonstrate that sulfur is evenly distributed in the framework of NMC. The nitrogen adsorption−desorption isotherms (Figure S5, Supporting Information) reveal a significant reduction of pore volume of NMC as a result of the filling of a large amount of elemental sulfur. However, there are still

dx.doi.org/10.1021/cs300791j | ACS Catal. 2013, 3, 862−870

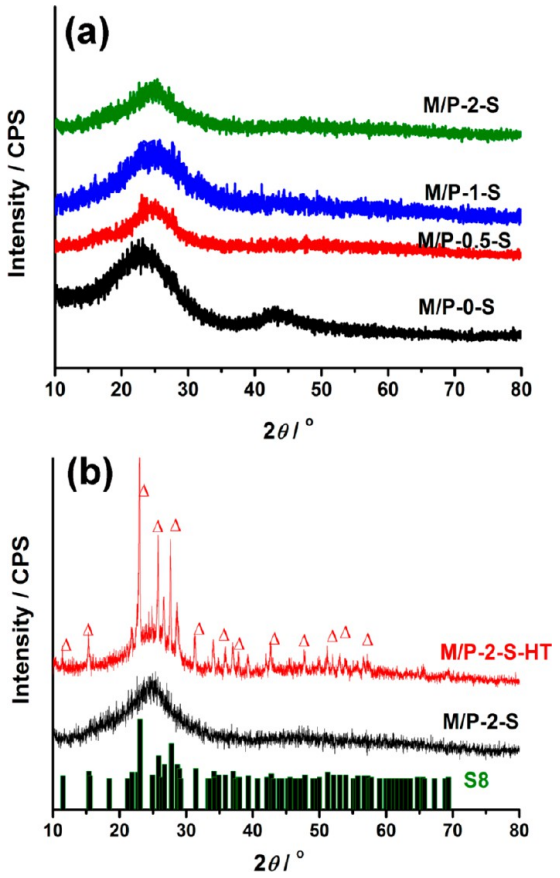

Figure 8. XRD patterns of the NMC after the oxidation of H_2S (a) and the exhausted M/P-2 before and after heat treatment at 120 °C.

considerable mesopores that are not fully utilized for the store of the product sulfur, suggesting there is room to further improve the capacity.

XRD analysis is conducted on the exhausted NMC composites, as shown in Figure 8a. There are almost no obvious differences between these samples; there is even a large amount of sulfur deposited into the M/P-1 and M/P-2. This result indicates that the product sulfur should be amorphous or that the sulfur atoms formed at 30 °C are unable to crystallize into a large size. However, mild heat treatment of the exhausted NMC (M/P-2-S) at 120 °C leads to the presence of intensity peaks corresponding to the polysulfides with the S_8 form, suggesting that the initial state of sulfur should be in the form of an ultrathin S_8 cluster. Further evidence for the production of elemental sulfur in our metal-free catalytic reaction is obtained by XPS spectra (Figure S6, Supporting Information) of the NMC after the oxidation.

3.4. Regeneration of the Exhausted NMC for H_2S Oxidation. The product sulfur deposited on the surface of the carbon framework can be easily removed by carbon disulfide (CS_2) scrubbing or thermal sublimation, leading to the NMC having very valuable recyclability. This is exemplified using CS_2 scrubbing as a regeneration method, which allows easy recovery of the product sulfur via vacuum rotary evaporation. During five regeneration tests, there is a slight decrease in catalytic activity of the NMC (M/P-2), retaining 95% ofthe initial sulfur capacity at the fifth run (Figure 9a). We further compare the structure and chemical nature of the fresh NMC with the regenerated NMC after five cycling tests. N_2 adsorption indicates that the porosity of the M/P-2 has no obvious changes after 5 regeneration tests (Figure 9b), indicating good structural stability of the NMC. However, elemental analysis reveals that the nitrogen content slightly decreases from 11.9 to

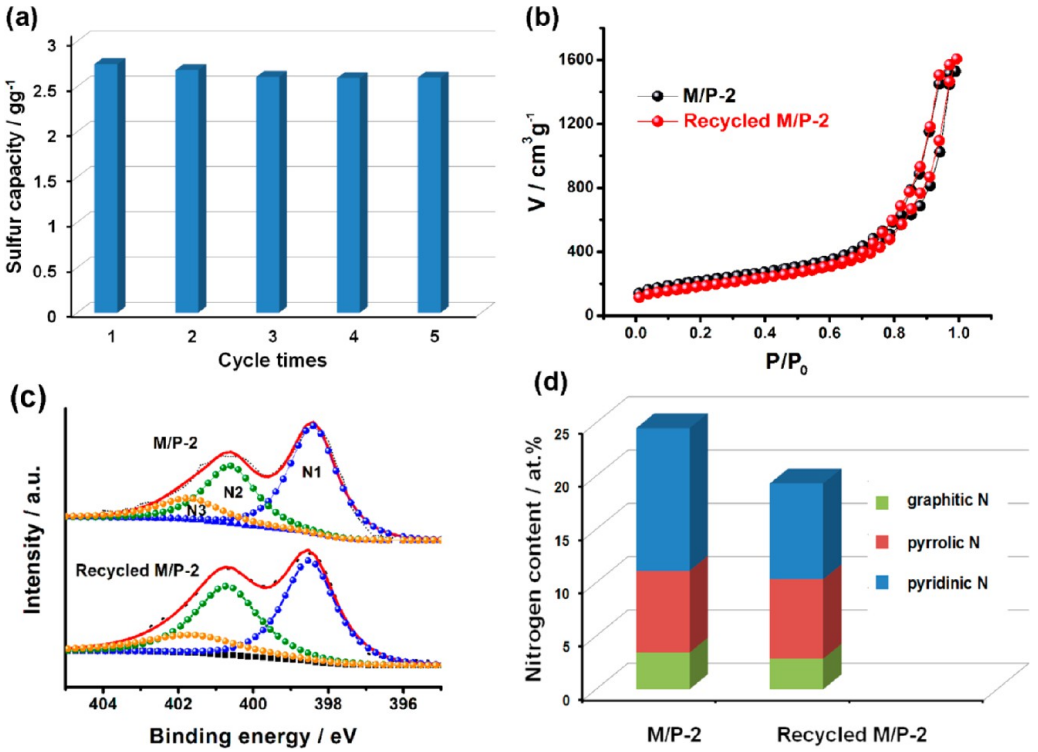

Figure 9. (a) Breakthrough sulfur capacities of NMC (M/P-2) recovered by CS_2 scrubbing. (b) N2 adsorption−desorption isotherms, (c) XPS N1s spectra and (d) the content of three nitrogen species of NMC (M/P-2) before and after five cycling tests.

dx.doi.org/10.1021/cs300791j | ACS Catal. 2013, 3, 862−870

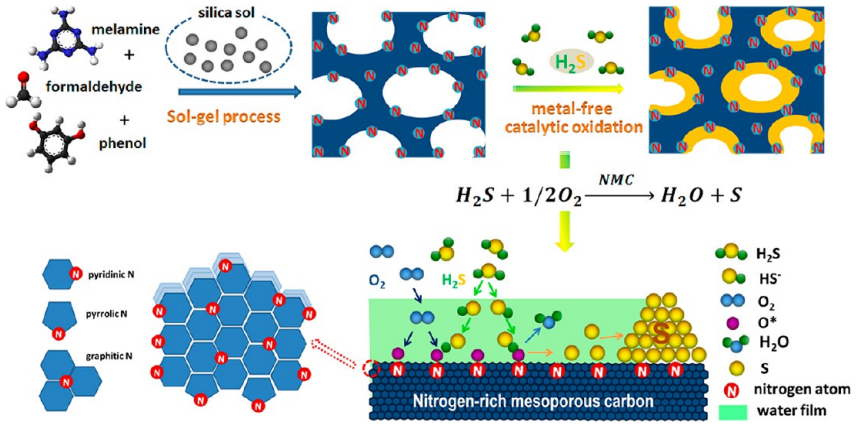

Figure 10. Schematic fabrication of NMC for the direct oxidation of H_2S and the possible reaction process.

10.2 wt % after 5 periods of oxidation reaction. XPS further demonstrates that the surface nitrogen atoms decrease from 24.5 to 19.3 at. % (Table S1, Supporting Information), which is mostly attributed to the loss of pyridinic nitrogen (Figure9d). Although there is a loss of a small portion of pyridinic nitrogen atoms, the good regeneration performance of NMC suggests that the major active nitrogen domains should be stable, which might be embedded inside the carbon framework and prevent the deactivation generally encountered with traditional supported catalysts. Thus, the regeneration of NMC lies at the heart of current efforts to render H_2S removal more sustainable, which has previously proved to be rather difficult. Research into regeneration by thermal sublimation, a more gentle technique than CS_2 scrubbing, is currently ongoing in our group.

3.5. Possible Reaction Mechanism of Metal-Free Catalytic Oxidation. It is apparent that a large number of nitrogen active sites helps to facilitate the high activity of the NMC toward the low-temperature catalytic oxidation of H_2S. On the basis of the vapor−liquid−solid mechanism for H_2S oxidation over the caustic catalysts,[11,38] we propose an overall mechanism to explain our observed results (Figure 10). Humidity is necessary for H_2S oxidation, which could form a thin water film on the surface of the carbon framework. H_2S molecules diffuse into the pores and dissolve into the water film. The presence of nitrogen groups as Lewis basic sites could increase the local basicity of the water film, which could facilitate the dissociation of H_2S into HS^- ions (pk 6.89). The nitrogen content in the NMC is highly critical because it dictates their basic properties, which determines the concentration of HS^- ions. Meanwhile, oxygen molecules diffuse into the pores and are preferentially adsorbed by the active sites, particularly those pyridinic nitrogen atoms at graphitic edge plane sites. The subsequent reaction between high concentration HS^- ions and adsorbed oxygen radicals leads to the formation of the elemental sulfur. Low operating temperatures would improve the catalytic activity by enhancing adsorption of the reactants as well as ensuring that undesirable side reactions would be minimized. The elemental sulfur produced in this way would be retained as a condensed phase within the mesopores, resulting in a slow deactivation of the NMC through active site occlusion. CS_2 scrubbing or thermal regeneration in nitrogen could then be employed to recover the elemental sulfur as product from the pores of the NMC, leaving the nitrogen active sites on the carbon framework exposed for the next use. Although partial loss of the nitrogen atoms occurs during the regeneration, the major active nitrogen atoms are stable enough to maintain long-term catalytic activity.

4. CONCLUSIONS

In conclusion, we demonstrate a cost-effective protocol to synthesize high-nitrogen-content mesoporous carbon desulfurizers using a colloidal silica nanocasting approach. The synthesis is very flexible and permits facile control of nitrogen content up to 10 wt %. Such high concentration of nitrogen basic sites on the carbon framework can greatly improve their catalytic activity toward H_2S oxidation at low temperature. Unparalleled sulfur capacity, high selectivity, and facile recovery are achieved for these inexpensive carbon materials, making them promising for large-scale industrial H_2S removal. From a broader perspective, these nitrogen-rich mesoporous carbons are a suitable metal-free catalyst for facilitating a wide range of transformations and may offer potential in pollution control and energy storage like supercapacitors and fuel cells.

■ ASSOCIATED CONTENT

Ⓢ Supporting Information

More results, including TEM and SEM images, TG, N_2 adsorption, and XPS results. This material is available free of charge via the Internet at http://pubs.acs.org.

■ AUTHOR INFORMATION

Corresponding Author

*Phone: +86 21 64252924. Fax: +86 21 64252914. E-mail: longdh@mail.ecust.edu.cn.

Author Contributions

‡These authors contributed equally.

Notes

The authors declare no competing financial interest.

■ ACKNOWLEDGMENTS

This work was supported in part by the National Science Foundation of China (Nos. 51172071, 51272077), and the Fundamental Research Funds for the Central Universities and Shanghai Pujiang Program.

■ REFERENCES

(1) Ghosh, T. K.; Toleffson, E. L. *Can. J. Chem. Eng.* **1986**, *64*, 960−968.

(2) Jou, F. Y.; Mather, A. E.; Otto, F. D. *Ind. Eng. Chem. Process Des. Dev.* **1982**, *21*, 539−544.

(3) Pieplu, A.; Saur, O.; Lavalley, J. C.; Legendre, O.; Nedez, C. *Catal. Rev. Sci .Eng.* **1998**, *40*, 409−450.
(4) Duan, H.; Yan, R. L.; Koe, C. C.; Wang, X. *Chemosphere* **2007**, *66*, 1684−1691.
(5) Seredych, M.; Bandosz, T. J. *Ind. Eng. Chem. Res.* **2006**, *45*, 3658−3665.
(6) Primavera, A.; Trovarelli, A.; Andreussi, P.; Dolcetti, G. *Appl. Catal., A* **1998**, *173*, 185−192.
(7) Wieckowska, J. *Catal. Today* **1995**, *24*, 405−465.
(8) Boki, K.; Tanada, S. *Chem. Pharm. Bull.* **1980**, *28*, 1270−1275.
(9) Meeyoo, V.; Lee, J. H.; Trimm, D. L.; Cant, N. W. *Catal. Today* **1998**, *44*, 67−72.
(10) Bagreev, A.; Bandosz, T. J. *J. Phys. Chem. B* **2000**, *104*, 8841−8847.
(11) Bandosz, T. J. *J. Colloid Interface Sci.* **2002**, *246*, 1−20.
(12) Bandosz, T. J. In *Carbon Materials for Catalysis*; Serp, P., Figueiredo, J. L., Eds.; John Wiley & Sons, Inc.: Hoboken, 2008; Chapter 2.
(13) Avgul, N. N.; Kiselev, A. V. In *Chemistry and Physics of Carbon*; Walker, P. L., Jr., Ed.; Marcel Dekker: New York, 1970; Vol. *6*.
(14) Turk, A.; Sakalis, S.; Lessuck, J.; Karamitsos, H.; Rago, O. *Environ. Sci. Technol.* **1989**, *23*, 1242−1245.
(15) Bandosz, T. J.; Lee, Q. *Carbon* **1998**, *36*, 39−44.
(16) Bandosz, T. J.; Baggreev, A.; Adib, F.; Turk, A. *Environ. Sci. Technol.* **2000**, *34*, 1069−1074.
(17) Chen, Q. J.; Wang, Z.; Long, D. H.; Liu, X. J.; Zhan, L.; Liang, X. Y.; Qiao, W. M.; Ling, L. C. *Ind. Eng. Chem. Res.* **2010**, *49*, 3152−3159.
(18) Long, D. H.; Chen, Q. J.; Qiao, W. M.; Zhan, L.; Liang, X. Y.; Ling, L. C. *Chem. Commun.* **2009**, *26*, 3898−3900.
(19) Chen, Q. J.; Long, D. H.; Wang, Z.; Liu, X. J.; Qiao, W. M.; Ling, L. C. *Microporous Mesoporous Mater.* **2011**, *142*, 641−648.
(20) Wu, Z. X.; Webley, P. A.; Zhao, D. Y. *J. Mater. Chem.* **2012**, *22*, 11379−11389.
(21) Jin, C.; Nagaiah, T. C.; Xia, W.; Spliethoff, B.; Wang, S.; Bron, M.; Schuhmann, W.; Muhler, M. *Nanoscale* **2011**, *2*, 981−987.
(22) Yang, S. B.; Feng, X. L.; Wang, X. C.; Mullen, K. *Angew. Chem., Int. Ed.* **2011**, *50*, 5339−5343.
(23) Ewels, C. P.; Glerup, M. *J. Nanosci. Nanotechnol.* **2005**, *5*, 1345−1363.
(24) Shao, Y.; Sui, J.; Yin, G.; Gao, Y. *Appl. Catal., B* **2008**, *79*, 89−99.
(25) Gong, K. P.; Du, F.; Xia, Z. H.; Durstock, M.; Dai, L. M. *Science* **2009**, *323*, 760−764.
(26) Bandosz, T. J. *Carbon* **1999**, *37*, 483−491.
(27) Adib, F.; Bagreev, A.; Bandosz, T. J. *Langmuir* **2000**, *16*, 1980−1986.
(28) Bagreev, A.; Menendez, J. A.; Dukhno, I.; Tarasenko, Y.; Bandosz, T. J. *Carbon* **2004**, *42*, 469−476.
(29) Wang, J. T.; Chen, Q. J.; Liu, X. J.; Qiao, W. M.; Long, D. H.; Ling, L. C. *Mater. Chem. Phys.* **2011**, *129*, 1035−1041.
(30) Boyd, K. J.; Marton, D.; Todorov, S. S.; Al-Bayati, A. H.; Kulik, J.; Zuhr, R. A.; Rabalais, J. W. *J. Vac. Sci. Technol., A* **1995**, *13*, 2110−2122.
(31) Dementjev, A. P.; de Graaf, A.; van de Sanden, M. C. M.; Maslakov, K. I.; Naumkin, A. V.; Serov, A. A. *Diamond Relat. Mater.* **2000**, *9*, 1904−1907.
(32) Qu, L. T.; Liu, Y.; Baek, J. B.; Dai, L. M. *ACS Nano* **2010**, *4*, 1321−1326.
(33) Liu, R. L.; Wu, D. Q.; Feng, X. L.; Mullem, K. *Angew. Chem., Int. Ed.* **2010**, *49*, 2565−2569.
(34) Jaouen, F.; Lefevre, M.; Dodelet, J. P.; Cai, M. *J. Phys. Chem. B* **2006**, *110*, 5553−5558.
(35) Groenewolt, M.; Antonietti, M. *Adv. Mater.* **2005**, *17*, 1789−1792.
(36) Lai, L.; Potts, J. R.; Zhan, D.; Wang, L.; Tang, C. K.; Poh, C.; Gong, H.; Shen, Z.; Lin, J.; Ruoff, R. S. *Energy Environ. Sci.* **2012**, *5*, 7936−7942.
(37) Mochida, I.; Korai, Y.; Shirahama, M.; Kawano, S.; Hada, T.; Seo, Y.; Yoshikawa, M.; Yasutake, A. *Carbon* **2000**, *38*, 227−239.
(38) Bagreev, A.; Bandosz, T. J. *Ind. Eng. Chem. Res.* **2005**, *44*, 530−538.